PAPER

2-Nitrophenol sensor-based wet-chemically prepared binary doped Co₃O₄/Al₂O₃ nanosheets by an electrochemical approach†

Mohammed M. Rahman, [ID] [ab] M. M. Alam [ID] *[c] and Abdullah M. Asiri [ID] [ab]

Herein, the wet-chemical process (co-precipitation) was used to prepare nanosheets (NSs) of Co₃O₄/Al₂O₃ in an alkaline medium (pH ∼ 10.5). The synthesized NSs were totally characterized by Fourier-transform infrared spectroscopy (FTIR), ultraviolet visible spectroscopy (UV/vis), field emission scanning electron microscopy (FESEM), energy-dispersive X-ray spectroscopy (EDS), X-ray photoelectron spectroscopy (XPS), and powder X-ray diffraction (XRD). The synthesized NSs were deposited onto a glassy carbon electrode (GCE) to prepare a very thin layer with a conducting binder for detecting 2-nitrophenol (2-NP) selectively by a reliable electrochemical method. The proposed chemical sensor exhibits good sensitivity (54.9842 μA μM⁻¹ cm⁻²), long-term stability, and enhanced chemical response by electrochemical approaches. The resultant current is found to be linear over the concentration range (LDR) from 0.01 nM to 0.01 mM. The estimated detection limit (DL) is equal to 1.73 ± 0.02 pM. This study introduces a potential route for future sensitive sensor development with Co₃O₄/Al₂O₃ NSs by an electrochemical approach for the selective detection of hazardous and carcinogenic chemicals in environmental and health care fields.

1. Introduction

Nitro-organic compounds (nitro-phenols) are well known as anthropogenic, toxic, inhibitory, and bio-refractory compounds and have vast industrial applications in the manufacture of a variety of useful products such as pharmaceuticals, industrial chemicals, pesticides, organic dyes, fungicides, insecticides, explosives, and aniline.[1] Therefore, the EPA (Environmental Protection Agency) and EU (European Union) have enlisted NPs as hazardous because of their highly toxic behavior towards the environment including human, animal, plants, aquatic life, and living organisms.[2–4] NPs may cause various harmful effects in human body, particularly cancer, generate poisoning, and tumors in the urinary tract.[5,6] The NPs are soluble in water, and due to the numerous manmade activities, they have not only been detected in industrial effluents, but also in fresh water and marine environment.[7] To protect the public health and the environment from harmful effects of NPs, it is obligatory to develop an efficient and sensitive portable device (chemical sensor) that will be used to detect NPs in the working place, environment, and public health sector.[8] The existing typical methods, such as spectrophotometry,[9] fluorescence,[10] gas chromatography,[11] capillary electrophoresis,[12] and high performance liquid chromatography,[13] are applied to detect NPs. However, these traditional methods have several disadvantages such as being costly and time consuming, requiring heavy instrumentation, and are complicated to use outdoors. On the other hand, the electrochemical method has useful features including low cost, easy operation, short response time, portable simple instrumentation, and selectivity with high sensitivity.[14]

The transition metal oxides with multiple oxidation states such as Fe₂O₃, Co₃O₄, MnO₂, and CrO₂ are extensively applied as a successive electron mediators to detect NPs.[15] An efficient NP chemical sensor fabricated with α-MnO₂ nanotubes had exhibited the sensitivity of 19.18 μA mM⁻¹ cm⁻² and detection limit of 0.1 mM.[16] Another NP chemical sensor based on Mn₂O₃/ZnO nanoparticles showed the sensitivity 4.6667 μA μM⁻¹ cm⁻² with the detection limit 0.83 nM.[17] In this decade, carbon nanotubes impregnated with transition metal oxides are extensively considered for the detection of environmental toxins, and this is becoming increasingly popular ever since the first invention.[18–20] It has been reported that the NP sensor fabricated with hydride components of carbon nanotube and phthalocyanine cobalt(ɪɪ) shows an outstanding detection limit 0.2 μM with a linear dynamic range from 1 μM to 1.9 mM.[21] Besides this, another talented NP chemical sensor assembled

ᵃChemistry Department, King Abdulaziz University, Faculty of Science, P.O. Box 80203, Jeddah 21589, Saudi Arabia

ᵇCenter of Excellence for Advanced Material Research (CEAMR), King Abdulaziz University, P.O. Box 80203, Jeddah 21589, Saudi Arabia

ᶜDepartment of Chemical Engineering and Polymer Science, Shahjalal University of Science and Technology, Sylhet 3100, Bangladesh. E-mail: mmalamsust@gmail.com; Tel: +880-821548976

† Electronic supplementary information (ESI) available. See DOI: 10.1039/c7ra10866d

with a poly(diallyldimethylammonium chloride)-functionalized graphene composite has exhibited a dynamic result of detection limit 0.02 μM with a wider linear dynamic range from 0.06 to 110 μM.[22]

Due to the high toxicity of 2-NP, sustainable development of methods for its selective detection is urgently needed. Therefore, an initiative has been taken for efficient detection of 2-NP by an electrochemical sensor constructed with Co_3O_4/Al_2O_3 NSs. A thin layer of Co_3O_4/Al_2O_3 NSs with a conducting binding agent (5% Nafion suspension in ethanol) was deposited on GCE to obtain a working electrode of 2-NP chemical sensor. The assembled Co_3O_4/Al_2O_3 NS/binder/GCE was applied successfully to detect 2-NP by a reliable electrochemical approach. To the best of our knowledge, the exploration of environmental toxin (2-NP) using a chemical sensor fabricated with active Co_3O_4/Al_2O_3 NSs has been reported for the first time herein. Therefore, it may be concluded that the 2-NP chemical sensor based on Co_3O_4/Al_2O_3 NSs onto GCE is a novel introduction in the field of sensor technology with promising applications in environmental toxin analysis.
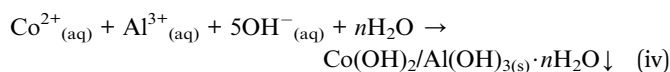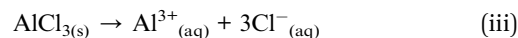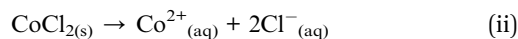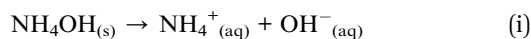
2.   Experimental

2.1   Materials and methods

The analytical grade chemicals cobalt(II) chloride ($CoCl_2$), aluminum chloride ($AlCl_3$), and ammonium hydroxide (NH_4OH) were obtained from the Sigma-Aldrich company and used as received to prepare Co_3O_4/Al_2O_3 NSs. To execute this study, M-tolylhydrazine (M-THyd), 2,4-dinitrophenol (2,4-DNP), 2-nitrophenol (2-NP), methanol (M), 3-methylaniline (3-MA), 3-chlorophenol (3-CP), ammonium hydroxide (AH), 3,4-diaminotoluene (3,4-DAT), 3-methoxyphenylhydrazine (3-MPHyd), bisphenol A (BPA), Nafion (5% Nafion suspension in ethanol), monosodium phosphate, and disodium phosphate were purchased from Sigma-Aldrich company. To explore the FTIR and UV-vis spectra, the produced Co_3O_4/Al_2O_3 NSs were analyzed using a Thermoscientific NICOLET iS50 FTIR (Madison, WI, USA) and 300 UV/visible spectrophotometer (Thermoscientific), respectively. The binding energies of Co, Al, and O and the corresponding oxidation states were measured by XPS analysis using a K-α1 spectrometer (thermo scientific, K-α1 1066) with a radiation source (A1Kα1, Beam spot size = 300.0 μm, pass energy = 200.0 eV, and pressure ∼ 10^{-8} torr). The optical properties, such as the arrangement of molecules, analysis of elements, morphological structure, and particle size, of synthesized NSs were investigated by implementation of FESEM (JEOL, JSM-7600F, Japan) and XEDS. Besides this, the phase (crystallinity of nanoparticles) identification was carried out by the execution of XRD analysis on the prepared Co_3O_4/Al_2O_3 NSs under ambient conditions. A slurry of NSs was used to coat the GCE with a conducting binder, and the resulting working electrode was implemented successfully to detect 2-NP in an aqueous medium. The electrochemical measurement was executed by a Keithley electrometer (6517A, USA) under room condition.
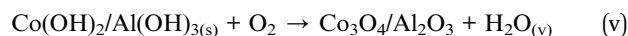
2.2   Preparation of Co_3O_4/Al_2O_3 NSs by a wet-chemical process

The wet-chemical process (co-precipitation) is an extensively used technique to prepare doped nanomaterials at low temperatures. This method involves three successive steps: (i) precipitation of two or more metal hydroxides in aqueous media, (ii) drying of separated precipitate, and (iii) calcination of dried precipitate in a high temperature muffle furnace. For the execution of this study, the predetermined weights of cobalt chloride ($CoCl_2$) and aluminum chloride ($AlCl_3$) were dissolved in 100.0 mL de-ionized (DI) water in a 250.0 mL conical flask. Then, a 0.1 M solution of NH_4OH was added to the resultant solution dropwise under continuous magnetic stirring, and the pH of the solution was adjusted to around 10.5. Under this condition, the metal ions were precipitated out quantitatively in the form of $Co(OH)_2/Al(OH)_3$. The precipitate was separated out from water and then dried in an oven at 105 °C. Subsequently the dried sample was calcined at 500 °C for 6 hours in a high temperature furnace for the metal hydroxides to transform into the metal oxide form Co_3O_4/Al_2O_3 in presence of atmospheric oxygen. The calcined sample in the oxide form was ground in a mortar into nanosized particles. The reaction scheme is supposed to be as follows:

In aqueous medium:

$$NH_4OH_{(s)} \rightarrow NH_4^+{}_{(aq)} + OH^-{}_{(aq)} \qquad (i)$$

$$CoCl_{2(s)} \rightarrow Co^{2+}{}_{(aq)} + 2Cl^-{}_{(aq)} \qquad (ii)$$

$$AlCl_{3(s)} \rightarrow Al^{3+}{}_{(aq)} + 3Cl^-{}_{(aq)} \qquad (iii)$$

$$Co^{2+}{}_{(aq)} + Al^{3+}{}_{(aq)} + 5OH^-{}_{(aq)} + nH_2O \rightarrow$$
$$Co(OH)_2/Al(OH)_{3(s)} \cdot nH_2O \downarrow \qquad (iv)$$

In the muffle furnace:

$$Co(OH)_2/Al(OH)_{3(s)} + O_2 \rightarrow Co_3O_4/Al_2O_3 + H_2O_{(v)} \qquad (v)$$

In the wet-chemical process, the precipitation of metal ion in the form of metal hydroxide is dependent on the value of K_s (solubility product constant) in an aqueous medium. At the pH 10.5, the K_s values for $Al(OH)_3$ and $Co(OH)_2$ are 3×10^{-34} and 5.92×10^{-15}, respectively.[34] As 0.1 M ammonium hydroxide solution is added dropwise to the resultant solution, the OH^- concentration increases gradually. Consequently, with the lower K_s value of $Al(OH)_3$, aluminum hydroxide starts to precipitate first and forms nuclei of crystals.[23] Then, with an increase in the OH^- ion concentration, the crystallites of aluminum hydroxide start to aggregate. Due to the addition of ammonium hydroxide in the resulting solution, the pH continues to increase for the adjustment of the reactor during preparation of nanomaterials. Then, cobalt hydroxide also starts to precipitate, which is adsorbed on crystallites of aluminum hydroxide. This similar tendency of growth pattern of nanomaterials has been reported elsewhere.[24–26] Subsequently, the obtained crystals of metal hydroxides are sequentially washed with water, ethanol, and acetone and dried overnight at 105 °C in an oven. After this, the

dried sample is subjected to calcination at higher temperatures in a furnace (Barnstead Thermolyne, 6000 Furnace, USA) at 500 °C for 6 hours. The schematic of the formation mechanism of Co_3O_4/Al_2O_3 NSs is presented in Scheme 1. To obtain the nano-sized particles, the calcined Co_3O_4/Al_2O_3 NSs were ground in a mortar. The prepared NSs were applied for the detection of 2-NP by an electrochemical approach under ambient conditions.

2.3 Fabrication of GCE with Co_3O_4/Al_2O_3 NSs

A slurry of Co_3O_4/Al_2O_3 NSs was prepared in ethanol and coated on a GCE as a very thin layer. To enhance the physical binding strength between NSs and GCE, a drop of Nafion (5% Nafion suspension in ethanol) was added. The assembled Co_3O_4/Al_2O_3 NS/binder/GCE was kept inside an oven at 34.0 °C for enough time to dry the conducting film entirely. The desired electrochemical cell was organized with the Co_3O_4/Al_2O_3NS/binder/ GCE and a Pt-wire (diameter 1.5 mm) as the working electrode and the counter electrode, respectively. To execute the sensor analytical performances, a series of 2-NP solutions based on the concentration ranging from 0.01 nM to 0.1 mM was prepared and used as a target analyte. The sensitivity of the anticipated chemical sensor was estimated from the slope of the calibration curve accomplished as resultant-current *versus* applied-concentration of 2-NP. The linear dynamic range (LDR) was measured from the maximum linearity (regression coefficient, r^2) of calibration curve, and detection limit was obtained from the signal to noise ratio of 3. The used electrometer is a simple two-electrodes system. The volume of the buffer solution (PBS) in the measuring electrochemical cell was maintained constant at 10.0 mL during the execution of this study.

3. Results and discussions

3.1 Structural analyses

The XRD (powder X-ray diffraction) patterns are able to provide detailed information about unit cell dimensions (phase crystallinity), and this technique was implemented on Co_3O_4/Al_2O_3 NSs with the radiation source Cu–Kα1 (λ = 1.54178 Å) in the range of 10–80°, and the corresponding scanning speed was $2°$ min^{-1}. According to the XRD spectrum presented in Fig. 1, the synthesized Co_3O_4/Al_2O_3 NSs contain well-assorted phases of Co_3O_4 and Al_2O_3. As observed from the Fig. 1, the reflected peaks of Co_3O_4 indices as β are (111), (220), (222), (400), (533), (622), (440), and (511), having great similarities with the previous reports.[27–30] Beside this, the observed diffracted peaks
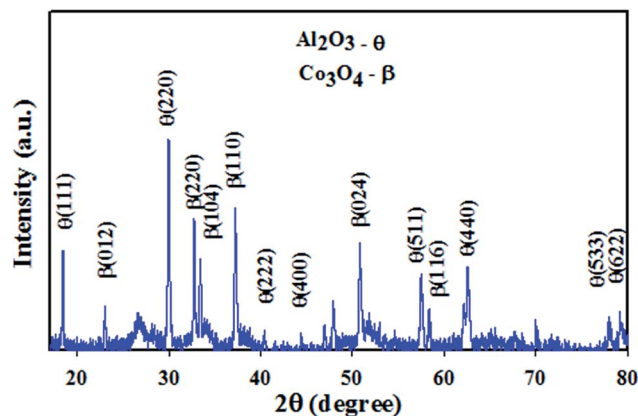

Fig. 1 Powder XRD pattern of the Co_3O_4/Al_2O_3 nanostructures for the structural analysis.

for Al_2O_3 indices as θ are (012), (104), (024), (220), (110), and (116), which have been identified by previous authors[31–35] and JCPDS no. 29-0063 to be belonging to Al_2O_3. Based on the Scherrer equation, the crystal size of the nanoparticles can be calculated from the XRD diffraction pattern.

$$D = 0.9l\lambda/(\beta \cos \theta) \qquad (vi)$$

Herein, λ represents the wavelength (X-ray radiation = 1.5418 Å) and β is full width at half maxima (FWHM), corresponding to most intense peak, and θ is the diffracting angle.[36] From the eqn (vi), the calculated crystal size (following the Scherrer equation) is equal to 30.86 nm. The optical analysis of Co_3O_4/Al_2O_3 NSs is also performed and presented in the ESI section (Fig. S4†).

3.2 Morphological and elemental analyses

The morphological and elemental analysis of synthesized Co_3O_4/Al_2O_3 NSs were investigated by FESEM and EDS analysis, as illustrated in Fig. 2. The typical FESEM images with high to low magnification are presented in the Fig. 2(a and b), and it is clearly visible that the synthesized Co_3O_4/Al_2O_3 materials are nanosheets in terms of shape.[37–39] The FESEM investigation is similar with the results of EDS analysis, as shown in Fig. 2(c and d). According to the EDS analysis, the composition of Co_3O_4/Al_2O_3 NSs is O 46.95%, Al 19.74%, and Co 33.3%. Besides these, any other peak is not visible; therefore, it can be concluded that the prepared Co_3O_4/Al_2O_3 NSs consist of cobalt, aluminum, and oxygen only.[40–42]

3.3 Binding energy analysis

The synthesized NSs were subjected to XPS investigation with an X-ray beam. The XPS spectrum is obtained when the atoms of the sample absorb the kinetic energy of X-ray beam and the electrons of outer spin orbital jump from lower to higher energy level. The atomic composition with the corresponding chemical formula and the oxidation state of the species present in the nanomaterial can be scrutinized efficiently by this practice.[43–45] The core level XPS spectra of Co 2p, Al 2p, and O 1s are presented in Fig. 3. The high resolution of Co 2p spectrum shows
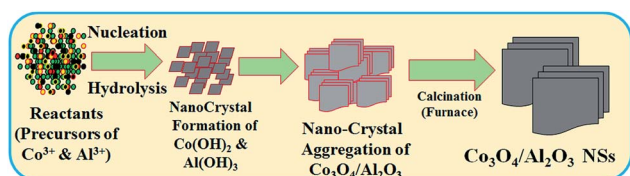
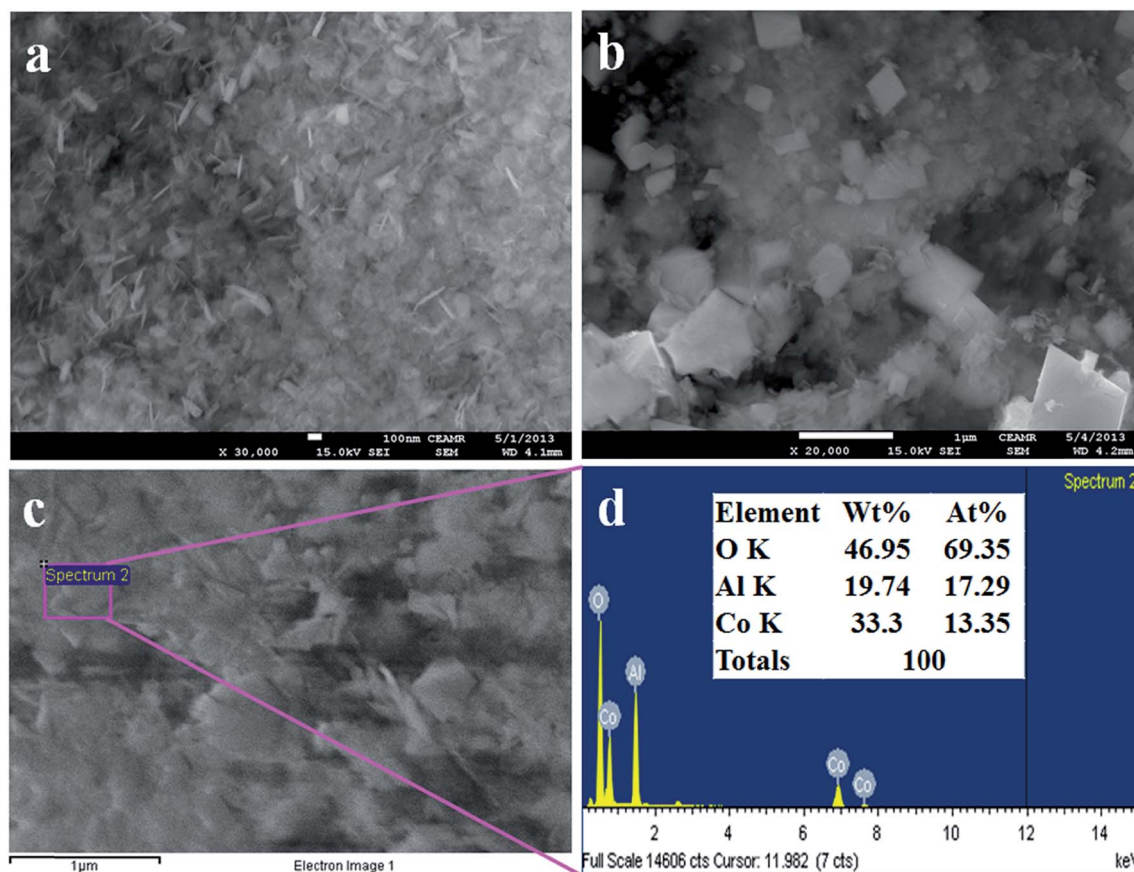Scheme 1 The growth mechanism of Co_3O_4/Al_2O_3 NSs produced by the low-temperature wet-chemical method.

Fig. 2 Morphological and elemental analyses (a and b) FESEM analysis from high to low magnified images and (c and d) elemental analysis of Co_3O_4/Al_2O_3 nanostructures.

two obvious dominated peaks centered at 781.0 and 796.0 eV. These two sharp peaks can be ascribed to Co $2p_{3/2}$ and Co $2p_{1/2}$ orbits and obviously verify the presence of Co^{3+}. The projected two satellite peaks of Co $2p_{3/2}$ and Co $2p_{1/2}$ are at 787.0 and 803.0 eV, respectively. These two peaks can be attributed to the presence of Co^{2+} in the synthesized NSs, as illustrated in Fig. 3(c).[46–50] Therefore, the presence of dominant and satellite peaks of Co 2p spin orbitals indicate the co-existence of Co(II) and Co(III) on the surface of synthesized Co_3O_4/Al_2O_3 NSs. The O 1s exhibit a peak at 531.3 eV, which is presented in Fig. 3(b) and attributed to O^{2-} in Al_2O_3.[51–55] The XPS spectra of Al 2p is concentrated at 73.3 and 75.1 eV, and the peaks of Al 2p at 75.1 eV are ascribed to $Al^{3+}–O^{2-}$ bonds in Al_2O_3, as illustrated in Fig. 3(d).[56–59] The different states of O 1s, Al 2p, and Co 2p are also quantified and presented in the ESI section (Fig. S5†).

3.4 Applications: sensing of 2-NP by Co_3O_4/Al_2O_3 NSs

The selective detection of 2-NP was executed in the optimized buffer system, and this performance was carried out by the implementation of Co_3O_4/Al_2O_3 NS/binder/GCE as the working electrode. To enhance the binding strength between NSs and GCE, a drop of Nafion was added. Nafion not only enhances the binding strength, but also increases stability, conductivity, and electron transfer rate of the electrode.[60,61] Thus, the prepared

electrode exhibited the advantages of high stability in air as well as in chemical environment, enhanced electrochemical performance during the detection of target analyte (2-NP), and can be easily subjected to performances, assembling, and fabrication, and above all, safe chemo-characteristics. Therefore, the proposed chemical sensor Co_3O_4/Al_2O_3 NS/binder/GCE was successfully used to detect 2-NP in an aqueous medium. During the performance of 2-NP chemical sensor, applied $I–V$ was measured on thin-film of Co_3O_4/Al_2O_3 NS/binder/GCE, and the holding time in the electrometer was set as 1.0 s. A possible reduction mechanism of 2-NP is illustrated in Scheme 2. As observed from Scheme 2, the electrons are accepted from the applied current to reduce 2-NP into 2-AP (2-aminophenol). Therefore, the species of reactive 2-NP are adsorbed on the Co_3O_4/Al_2O_3 NS surface and reduced to 2-aminophenol, as shown in reaction (vii) to (ix). Since the electrons are required to reduce 2-NP, the electrochemical response ($I–V$) is inversely proportional to the corresponding concentration of 2-NP.[62–65] A schematic of the detection process of 2-NP based on Co_3O_4/Al_2O_3 NS/binder/GCE sensor is demonstrated in Scheme 2.

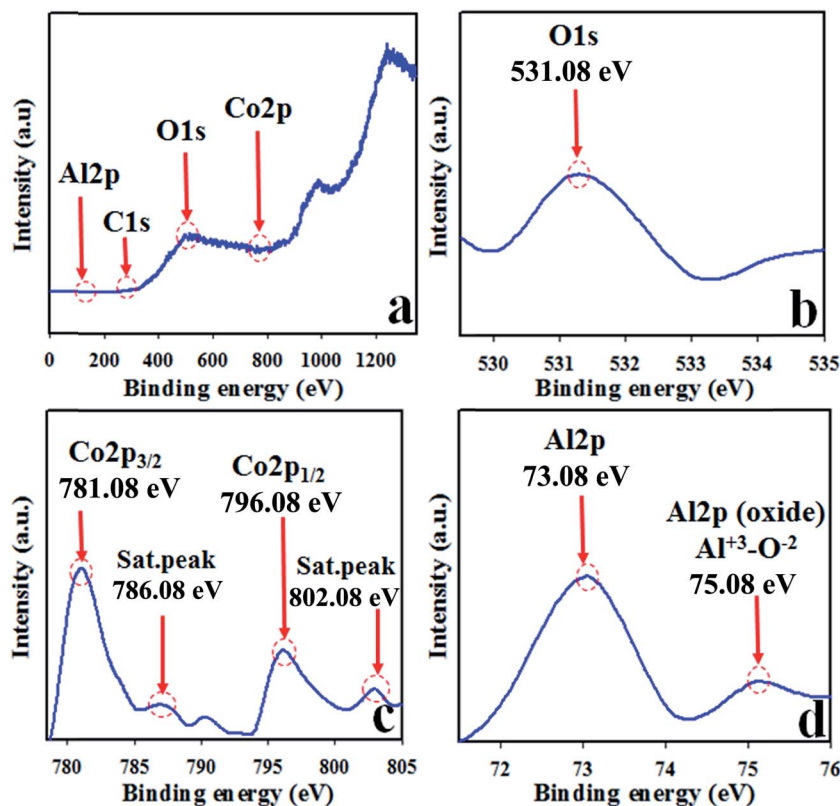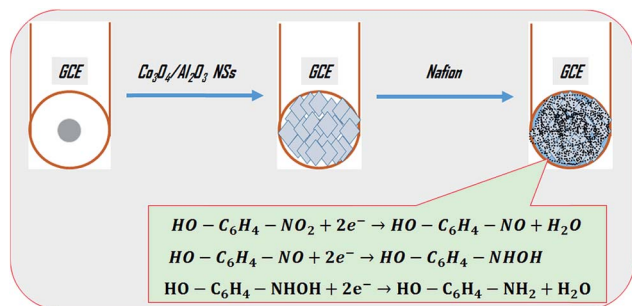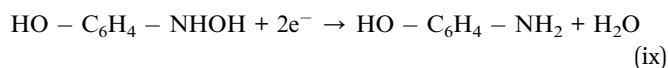The possible suggested reduction mechanism of 2-NP is presented in the reaction (vii) and (ix).
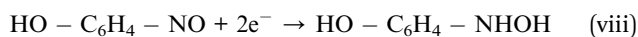
$$HO - C_6H_4 - NO_2 + 2e^- \rightarrow HO - C_6H_4 - NO + H_2O \quad (vii)$$
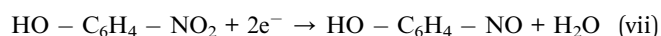
Fig. 3 Binding energy analysis by XPS study of Co_3O_4/Al_2O_3 NSs (a) full spectrum, (b) O 1s level, (c) spin orbit Co 2p level, and (d) spin orbit of Al 2p level.

Scheme 2 The expected sensing mechanism for the determination of 2-NP by Co_3O_4/Al_2O_3 NSs on sensor probe.

$$HO - C_6H_4 - NO + 2e^- \rightarrow HO - C_6H_4 - NHOH \quad \text{(viii)}$$

$$HO - C_6H_4 - NHOH + 2e^- \rightarrow HO - C_6H_4 - NH_2 + H_2O \quad \text{(ix)}$$

The synthesized NSs are not responsive equally in all buffers to applied *I–V*. Therefore, for obtaining the maximum output of the *I–V* responses, the pH of the measuring buffer system was necessary to be optimized for the Co_3O_4/Al_2O_3 NS/binder/GCE. Fig. 4(a) represents the *I–V* response of pH ranging from 5.7 to 8.0. Obviously, among the tested buffer system, the best *I–V* response was attained at pH 6.5. Then, a number of environmental toxins have been investigated at the concentration level of 1.0 μM and pH =

7.5 with the proposed chemical sensor. The electrochemical responses of M-THyd, 2,4-DNP, 2-NP, methanol, 3-MA, 3-CP, AH, 3,4-DAT, 3-MPHyd, and BPA are illustrated in Fig. 4(b). Obviously, the electrochemical response of 2-NP has the highest intensity under experimental conditions. The reproducibility test of a chemical sensor provides the evidence of reliability. Therefore, this test was performed at 0.1 μM concentration of 2-NP, and the resulting data is represented in Fig. 4(c). As seen in the Fig. 4(c), the replicated six runs are practically indistinguishable under an identical condition. The electrochemical responses are unchanged even after washing of electrode in each trial. Therefore, this test provides the evidence of reliability, and the projected 2-NP chemical sensor can be applied in the real field successively. The relative standard deviation of the reproducibility performances (RSD) is estimated, and it is found to be 1.54 at an applied potential of +1.5 V. The response time is another tool to measure the efficiency of a chemical sensor, and this test has been performed using a 0.1 μM solution of 2-NP. As illustrated in Fig. 4(d), steady response is achieved in about around 10.5 s, and the obtained result may be considered highly satisfactory.

Fig. 5(a) presents the *I–V* response of 2-NP for various concentrations ranging from 0.01 nM to 0.1 mM. Evidently, this is a very wide range, and the applied potential is higher than +1.0 V. As shown in Fig. 5(a), *I–V* responses are distinguishable from lower to higher concentration of 2-NP. To evaluate the analytical performance of the projected chemical sensor, the current data at an applied potential of +1.5 V has been obtained
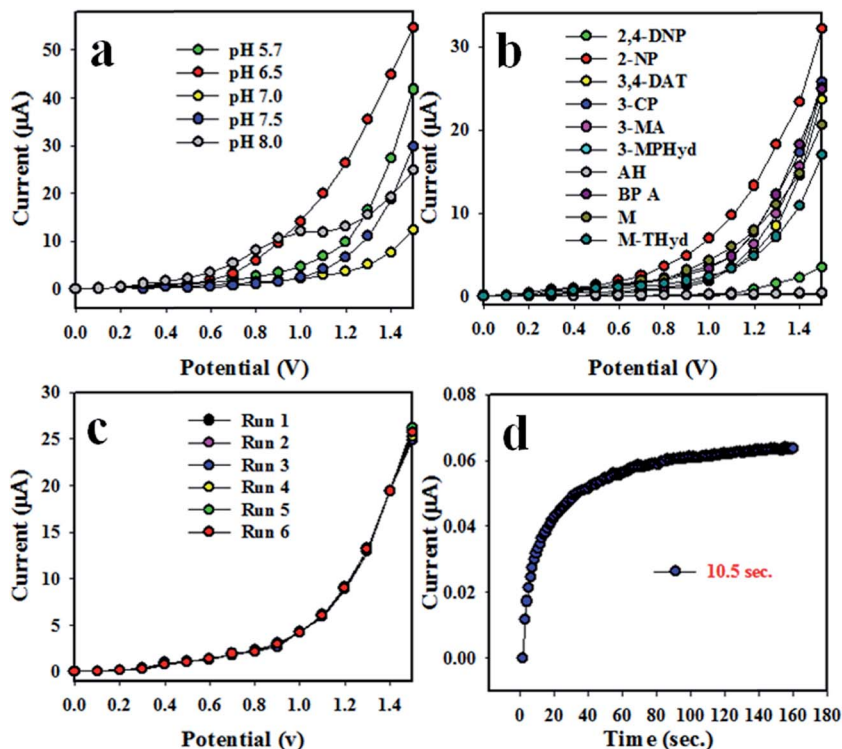
Fig. 4 Optimization of 2-NP with Co_3O_4/Al_2O_3 NSs. (a) pH optimization, (b) selectivity, (c) repeatability, and (d) response time.
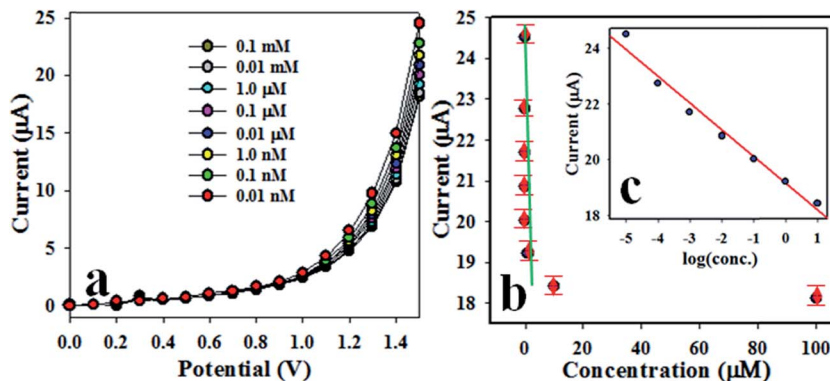

Fig. 5 Performance of 2-NP sensor. (a) Concentration variation of 2-NP based on Co_3O_4/Al_2O_3 NSs/GCE by $I-V$ method, (b) calibration curve (inset: log[2-NP conc.] *vs.* current).

from Fig. 5(a) and plotted as current *vs.* concentration of 2-NP in the Fig. 5(b), which is known as a calibration plot. This calibration plot is found to be linear with the regression co-efficient value $r^2 = 0.99$ along the *x*-axis in logarithmic scale. The sensitivity of 2-NP chemical sensor is estimated from the slope of calibration curve, and it is equal to 54.9842 $\mu A \ \mu M^{-1} \ cm^{-2}$. The linear dynamic range (LDR) is found to be from 0.01 nM to 0.01 mM. At a signal to noise ratio equal to 3, the limit of detection (LOD) and limit of quantity (LOQ) were calculated to be 1.73 ± 0.02 pM and 5.77 ± 0.02 pM, respectively. Obviously, the Co_3O_4/Al_2O_3 NS/binder/GCE electrode could be used to determine 2-NP in an aqueous medium in a wide concentration range. The stability performance of electrode based on $Co_3O_4/$

Al_2O_3 NSs has been evaluated in the detection of 2-NP under identical conditions for intra-days and inter-day, as presented in Fig. S1 and S2,† respectively, in the ESI section.† Therefore, it can be concluded from Fig. S1 and S2† that the fabricated electrode is able to perform efficiently in long-term. The reliable measurement of 2-NP with other toxins such as 3-CP and 4-NP in an aqueous medium is illustrated in Fig. S3 in the ESI.† According to this figure, the toxin 3-CP and 4-NP have not shown any remarkable interference effect on the projected chemical sensor during the sensing of 2-NP.

As observed from Fig. 5(a), the electrochemical response of 2-NP chemical sensor based on active Co_3O_4/Al_2O_3 NS/GCE increases with a decrease in the concentration of 2-NP.

Therefore, the highest I–V response is found at lowest concentrations of 2-NP. During the sensing of 2-NP by Co_3O_4/Al_2O_3 NS/GCE electrode, a small surface coverage due to the adsorption of few 2-NP molecules on surface of electrode occurs in the initial stage, and corresponding reduction reaction of 2-NP starts progressively. With enrichment of analyte (2-NP), the rate of reaction is increased, and the higher surface coverage is obtained. With further enrichment of 2-NP concentration in the sensing medium, the reduction reaction comes to equilibrium, and the surface coverage approaches its saturation state. With an additional increase in the analyte concentration, a steady state equilibrium I–V response is observed, and a saturated

surface coverage is accomplished. Therefore, it can be summarized that the proposed 2-NP chemical sensor based on the Co_3O_4/Al_2O_3 NS/GCE assembly can be applied for efficient detection of the targeted toxin (2-NP). As indicated, the proposed 2-NP chemical sensor exhibits reasonable short response time of around 10.5 s, and it should be mentioned that 10.5 s is needed by the 2-NP chemical sensor to attain steady state saturation. Since the proposed 2-NP chemical sensor demonstrates a high sensitivity of 54.9842 $\mu A\ \mu M^{-1}\ cm^{-2}$, it can be accredited that it has very good adsorption capacity and active catalytic decomposition ability.[66–70] The interference effect is studied in the presence of different phenolic compounds and their derivatives, such as 2-NP, 2,4-DNP, BPA, and 3-CP, under identical conditions, as presented in Table 1.

According to analytical performance, such as selectivity, detection limit, and dynamic linear range, of the chemical sensor, the proposed 2-NP chemical sensor fabricated based on Co_3O_4/Al_2O_3 NS/GCE showed a reasonably qualified performance as compared to the chemical sensors based on the various transition nanostructured metal oxides, and a comparison is illustrated in Table 2. In brief, the fabricated 2-NP chemical sensor is simple and efficient to detect 2-NP by applying current *versus* potential electro-chemical approaches. The sensing performance, such as detection limit (LD), linear dynamic range (LDR), and sensitivity, of earlier tested 2-NP

Table 1 Measurement of interference effect by Co_3O_4/Al_2O_3 NS/GCE

| Toxins | Observed current[a] (μA) at +1.5 V | | | | | |
	R_1	R_2	R_3	R_4	Average[b] (μA)	RSD[c] (%)
2-NP	26.756	26.298	25.839	26.347	26.310	1.42
2,4-DNP	3.699	3.613	3.527	3.643	3.621	1.98
BPA	22.839	23.137	22.410	21.981	22.592	2.23
3-CP	23.688	22.875	23.525	24.175	23.566	2.28

[a] Mean of four repeated (R) determination (signal to noise ratio 3) with Co_3O_4/Al_2O_3 NSs/GCE at 0.1 μM concentration. [b] The average observed current of the corresponding toxin. [c] Relative standard deviation value indicates precision among four repeated determinations.

Table 2 Comparative performances of various nanomaterials or nanocomposites fabricated electrode for the detection of 2-NP by electrochemical approaches[a]

Materials	LOD	LDR	Sensitivity	Ref.
Ag_2O NPs/AuE	0.19 μM	1.0 μM to 0.5 mM	0.0474 $\mu A\ \mu M^{-1}\ cm^{-2}$	70
CuO nanohybrides	0.67 nM	1.0 nM to 1.0 mM	0.045 $\mu A\ \mu M^{-1}\ cm^{-2}$	71
Spinel $ZnMn_2O_4$	20.0 μM	50.0 μM to 0.05 M	1.5 $\mu A\ \mu M^{-1}\ cm^{-2}$	72
B-doped diamond electrodes	8.4 mM	—	0.3943 $\mu A\ \mu M^{-1}\ cm^{-2}$	73
Mn_2O_3–ZnO NPs/AgE	0.83 nM	100 pM to 50.0 μM	0.6667 $\mu A\ \mu M^{-1}\ cm^{-2}$	74
Ce_2O_3 CNT NCs	60 pM	100 pM to 100 μM	0.0016 $\mu A\ \mu M^{-1}\ cm^{-2}$	75
Co_3O_4/Al_2O_3 NSs/GCE	1.73 ± 0.02 pM	0.01 nM to 0.01 mM	54.9842 $\mu A\ \mu M^{-1}\ cm^{-2}$	This work

[a] DL (detection limit), LDR (linear dynamic range), nM (nanomole), pM (picomole).

Table 3 Measured concentration of 2-NP analytes in real environmental samples

Sample	Added 2-NP concentration	Determined 2-NP concentration[a] by Co_3O_4/Al_2O_3 NSs/GCE	Recovery[b] (%)	RSD[c] (%) (n = 3)
Industrial effluent	0.100 μM	0.0991 μM	99.1	2.11
	0.100 μM	0.1032 μM	103.2	
	0.100 μM	0.1022 μM	102.2	
Plastic baby bottle	0.100 μM	0.1019 μM	101.9	0.83
	0.100 μM	0.1032 μM	103.2	
	0.100 μM	0.1035 μM	103.5	
	0.100 μM	0.1053 μM	105.3	
Sea water	0.100 μM	0.1059 μM	105.9	1.02
	0.100 μM	0.1074 μM	107.4	

[a] Mean of three repeated determinations (signal to noise ratio 3) with Co_3O_4/Al_2O_3 NSs/GCE. [b] Concentration of 2-NP determined/concentration taken. [c] Relative standard deviation value indicates precision among three repeated determinations.

chemical sensors are associated and summarized in Table 2.[70–75]

3.5 The analysis of a real sample

The proposed 2-NP chemical sensor based on Co_3O_4/Al_2O_3 NSs was employed for validation to detect and quantify 2-NP in real samples to test its applicability in practical field. The samples were obtained from various sources such as industrial effluent, extracts from PC baby-bottle, and seawater. The results of the analyses are presented in Table 3 and seem quite satisfactory.

4.   Conclusions

The reliable wet-chemical process was used to prepare NSs of Co_3O_4/Al_2O_3 at low temperature. Later, a thin layer of NSs was deposited onto GCE with a conducting binder to fabricate the working electrode for the 2-NP chemical sensor development. The calcined NSs were characterized by FESEM, EDS, XPS, FTIR, UV/vis, and XRD and applied to successively detect 2-NP in an aqueous medium. The proposed 2-NP chemical sensor based on Co_3O_4/Al_2O_3 NSs displayed higher sensitivity, lower detection limit, broad linear dynamic ranges, and selectivity towards 2-NP by reliable I–V method. The applied current to concentration of 2-NP is linear over the concentration range from 0.01 nM to 0.01 mM with a detection limit of 1.73 ± 0.02 pM, LOQ of 5.77 ± 0.02 pM, and sensitivity of 54.9842 μA μM^{-1} cm^{-2}. This approach introduced a well-organized route of efficient chemical sensor development for environmental pollutants in a broad scales.

Conflicts of interest

There are no conflicts to declare.

Acknowledgements

References

1 N. Bakhsh, M. M. Mirkalaei, M. H. Yousefi and S. Manochehri, Electrodeposition of Cobalt Oxide Nanostructure on the Glassy Carbon Electrode for Electrocatalytic Determination of para-Nitrophenol, *Electroanalysis*, 2014, **26**, 2716–2726.

2 J. Li, D. Kuang, Y. Feng, F. Zhang, Z. Xu and M. Liu, A graphene oxide-based electrochemical sensor for sensitive determination of 4-nitrophenol, *J. Hazard. Mater.*, 2012, **20**, 250–259.

3 P. Deng, Z. Xu, Y. Feng and J. Li, Electrocatalytic reduction and determination of p-nitrophenol on acetylene black paste electrode coated with salicylaldehyde-modified chitosan, *Sens. Actuators, B*, 2012, **168**, 381–389.

4 R. M. A. Tehrani, H. Ghadimi and S. A. Ghani, Electrochemical studies of two diphenols isomers at graphene nanosheet–poly(4-vinyl pyridine) composite modified electrode, *Sens. Actuators, B*, 2013, **177**, 612–619.

5 O. Pinrat, K. Boonkitpatarakul, W. Paisuwan, M. Sukwattanasinitt and A. Ajavakom, Glucopyranosyl-1,4-dihydropyridine as a new fluorescent chemosensor for selective detection of 2,4,6-trinitrophenol, *Analyst*, 2015, **140**, 1886–1893.

6 N. Venkatramaiah, M. Desisy, G. C. Rocha, P. Srikanth, F. A. A. Paz and J. P. C. Tome, Synthesis and photophysical characterization of dimethylamine-derived Zn(II) phthalocyanines: exploring their potential as selective chemosensors for trinitrophenol, *J. Mater. Chem. C*, 2015, **3**, 1056–1067.

7 Z. Liu, J. Du, C. Qiu, L. Huang, H. Ma, D. Shen and Y. Ding, Electrochemical sensor for detection of p-nitrophenol based on nanoporous gold, *Electrochem. Commun.*, 2009, **11**, 1365–1368.

8 P. Deng, Z. Xu, Y. Feng and J. Li, Electrocatalytic reduction and determination of p-nitrophenol on acetylene black paste electrode coated with salicylaldehyde-modified chitosan, *Sens. Actuators, B*, 2012, **168**, 381–389.

9 A. Niazi and A. Yazdanipour, Spectrophotometric simultaneous determination of nitrophenol isomers by orthogonal signal correction and partial least squares, *J. Hazard. Mater.*, 2007, **146**, 421–427.

10 W. Zhang and C. R. Wilson, Indirect fluorescent determination of selected nitro-aromatic and pharmaceutical compounds *via* UV-photolysis of 2-phenylbenzimidazole-5-sulfonate, *Talanta*, 2008, **74**, 1400–1407.

11 J. A. Padilla-Sánchez, P. Plaza-Bolanos, R. Romero-González, A. Garrido-Frenich and J. L. M. Vidal, Application of a quick, easy, cheap, effective, rugged and safe-based method for the simultaneous extraction of chlorophenols, alkylphenols, nitrophenols and cresols in agricultural soils, analyzed by using gas chromatography–triple quadrupole-mass spectrometry/mass spectrometry, *J. Chromatogr. A*, 2010, **1217**, 5724–5731.

12 X. Guo, Z. Wang and S. Zhou, The separation and determination of nitrophenol isomers by high-performance capillary zone electrophoresis, *Talanta*, 2004, **64**, 135–139.

13 D. Hofmann, F. Hartmann and H. Herrmann, Analysis of nitrophenols in cloud water with a miniaturized light-phase rotary perforator and HPLC-MS, *Anal. Bioanal. Chem.*, 2008, **391**, 161–169.

14 M. Abaker, G. N. Dar, A. Umar, S. A. Zaidi, A. A. Ibrahim, S. Baskoutas and A. Al-Hajry, CuO nanocubes based highly-sensitive 4-nitrophenol chemical sensor, *Sci. Adv. Mater.*, 2012, **4**, 1–8.

15 G. J. Soler-Illia, E. L. Crepaldi, D. Grosso and C. Sanchez, Block copolymer-templated mesoporous oxides, *Curr. Opin. Colloid Interface Sci.*, 2003, **8**, 109–126.

16 J. Wu, Q. Wang, A. Umar, S. Sun, L. Huang, J. Wang and Y. Gao, Highly sensitive p-nitrophenol chemical sensor

based on crystalline α-MnO₂ nanotubes, *New J. Chem.*, 2014, **38**, 4420–4426.

17 M. M. Rahman, G. Gruner, M. S. Al-Ghamdi, M. A. Daous, S. B. Khan and A. M. Asiri, Chemo-sensors development based on low-dimensional codoped Mn₂O₃-ZnO nanoparticles using flat-silver electrodes, *Chem. Cent. J.*, 2013, **7**, 60.

18 S. Iijima, Helical microtubules of graphitic carbon, *Nature*, 1991, **354**, 56–58.

19 H. X. Luo, Z. J. Shi and N. Q. Li, Investigation of the electrochemical and electrocatalytic behavior of single-wall carbon nanotube film on a glassy carbon electrode, *Anal. Chem.*, 2001, **73**, 915–920.

20 Z. H. Wang, Q. L. Liang and Y. M. Wang, Carbon nanotube-intercalated graphite electrodes for simultaneous determination of dopamine and serotonin in the presence of ascorbic acid, *J. Electroanal. Chem.*, 2003, **540**, 129–134.

21 H. Wu, L. Guo, J. Zhang, S. Miao, C. He, B. Wang, Y. Wu and Z. Chen, Polyelectrolyte-free layer by layer self-assembled multilayer films of cationic phthalocyanine cobalt(II) and carbon nanotube for the efficient detection of 4-nitrophenol, *Sens. Actuators, B*, 2016, **230**, 359–366.

22 D. Peng, J. Zhang, D. Qin, J. Chen, D. Shan and X. Lu, An electrochemical sensor based on polyelectrolyte-functionalized graphene for detection of 4-nitrophenol, *J. Electroanal. Chem.*, 2014, **734**, 1–6.

23 J. R. H. Ross, *Econometric methods for research in education*, Elsevier, 2011, vol. 1, p. 87.

24 M. M. Hussain, M. M. Rahman, A. M. Asiri and M. R. Awual, Non-enzymatic simultaneous detection of L-glutamic acid and uric acid using mesoporous Co₃O₄ nanosheets, *RSC Adv.*, 2016, **6**, 80511–80521.

25 M. M. Rahman, S. B. Khan, M. Faisal, M. A. Rub, A. O. Al-Youbi and A. M. Asiri, Electrochemical determination of olmesartan medoxomil using hydrothermally prepared nanoparticles composed SnO₂–Co₃O₄ nanocubes in tablet dosage forms, *Talanta*, 2012, **99**, 924–931.

26 M. M. Rahman, S. B. Khan, G. Gruner, M. S. Al-Ghamdid, M. A. Daouse and A. M. Asiri, Chloride ion sensors based on low-dimensional α-MnO₂–Co₃O₄ nanoparticles fabricated glassy carbon electrodes by simple *I–V* technique, *Electrochim. Acta*, 2013, **103**, 143–150.

27 D. U. Lee, B. J. Kim and Z. Chen, One-pot synthesis of a mesoporous NiCo₂O₄ nanoplatelet and graphene hybrid and its oxygen reduction and evolution activities as an efficient bi-functional electrocatalyst, *J. Mater. Chem. A*, 2013, **1**, 4754–4762.

28 V. Panwar, A. Al-Nafiey, A. Addad, B. Sieber, P. Roussel, R. Boukherroub and S. L. Jain, Magnetic Co₃O₄/reduced graphene oxide nanocomposite as a superior heterogeneous catalyst for one-pot oxidative esterification of aldehydes to methyl esters, *RSC Adv.*, 2015, **5**, 88567–88573.

29 T. H. Yoon and Y. J. Park, Carbon nanotube/Co₃O₄ composite for air electrode of lithium-air battery, *Nanoscale Res. Lett.*, 2012, **7**, 28.

30 K. S. Kim and Y. J. Park, Catalytic properties of Co₃O₄ nanoparticles for rechargeable Li/air batteries, *Nanoscale Res. Lett.*, 2012, **7**, 47.

31 Z. Gu, F. Liu, J. Y. Howe, M. P. Parantham and Z. Pan, Germanium-catalyzed hierarchical Al₂O₃ and SiO₂ nanowire bunch arrays, *Nanoscale*, 2009, **1**, 347–354.

32 H. J. Kim and S. M. Nam, High loading of nanostructured ceramics in polymer composite thick films by aerosol deposition, *Nanoscale Res. Lett.*, 2012, **7**, 92.

33 Z. Yang, J. Yu, C. Li, Y. Zhong, W. Xuan, Z. Ren, Q. Wang, Y. Dai and H. Wang, Preparation of textured porous Al₂O₃ ceramics by slip casting in a strong magnetic field and its mechanical properties, *Cryst. Res. Technol.*, 2015, **1**, 645–653.

34 J. Lian, J. Ma, X. Duan, T. Kim, H. Li and W. Zheng, One-step ionothermal synthesis of γ-Al₂O₃ mesoporous nanoflakes at low temperature, *Chem. Commun.*, 2010, **46**, 2650–2652.

35 B. Yazdani, F. Xu, I. Ahmad, X. Hou, Y. Xia and Y. Zhu, Tribological performance of Graphene/Carbon nanotube hybrid reinforced Al₂O₃ composites, *Sci. Rep.*, 2015, **5**, 11579.

36 R. Jenkins and R. L. Snyder, *Introduction to X-ray Powder Diffractometry*, John Wiley & Sons, 1994, vol. 138, pp. 750–950.

37 K. K. Naik, S. Kumar and C. S. Rout, Electrodeposited spinel NiCo₂O₄ nanosheet arrays for glucose sensing application, *RSC Adv.*, 2015, **5**, 74585–74591.

38 K. K. Naik, R. T. Khare, M. A. More, D. J. Late and C. S. Rout, Glucose sensing and low-threshold field emission from MnCo₂O₄ nanosheets, *RSC Adv.*, 2016, **6**, 29734–29740.

39 S. Liu, K. S. Hui, K. N. Hui, J. M. Yund and K. H. Kim, Vertically stacked bilayer CuCo₂O₄/MnCo₂O₄ heterostructures on functionalized graphite paper for high-performance electrochemical capacitors, *J. Mater. Chem. A*, 2016, **4**, 8061–8071.

40 S. Liu, S. C. Lee, U. Patil, I. Shackery, S. Kang, K. Zhang, J. H. Park, K. Y. Chung and S. C. Jun, Hierarchical MnCo-layered double hydroxides@ Ni(OH)₂ core–shell heterostructures as advanced electrodes for supercapacitors, *J. Mater. Chem. A*, 2017, **5**, 1043.

41 J. S. Lee, W. Kim, S. Cho, J. Jun, K. H. Choa and J. Jang, Multidimensional hybrid conductive nanoplate-based aptasensor for platelet-derived growth factor detection, *J. Mater. Chem. B*, 2016, **4**, 4447–4454.

42 X. Leng, S. Wei, Z. Jiang, J. Lian, G. Wang and Q. Jiang, Carbon-encapsulated Co₃O₄ nanoparticles as anode materials with super lithium storage performance, *Sci. Rep.*, 2015, **5**, 16629.

43 A. Celebioglu, S. Vempati, C. Ozgit-Akgun, N. Biyikliab and T. Uyar, Water-soluble non-polymeric electrospun cyclodextrin nanofiber template for the synthesis of metal oxide tubes by atomic layer deposition, *RSC Adv.*, 2014, **4**, 61698–61705.

44 Y. Tan, Q. Gao, C. Yang, K. Yang, W. Tian and L. Zhu, One-dimensional porous nanofibers of Co₃O₄ on the carbon matrix from human hair with superior lithium ion storage performance, *Sci. Rep.*, 2015, **5**, 12382.

45 M. Alevli, C. Ozgit, I. Donmez and N. Biyikli, The influence of N₂/H₂ and ammonia N source materials on optical and

structural properties of AlN films grown by plasma enhanced atomic layer deposition, *J. Cryst. Growth*, 2011, **335**, 51–57.

46 J. Cui, X. Zhang, L. Tong, J. Luo, Y. Wang, Y. Zhang, K. Xiea and Y. Wu, A facile synthesis of mesoporous Co_3O_4/CeO_2 hybrid nanowire arrays for high performance supercapacitors, *J. Mater. Chem. A*, 2015, **3**, 10425–10431.

47 A. Younis, D. Chu, X. Lin, J. Lee and S. Li, Bipolar resistive switching in p-type Co_3O_4 nanosheets prepared by electrochemical deposition, *Nanoscale Res. Lett.*, 2013, **8**, 36.

48 H. Xia, D. Zhu, Z. Luo, Y. Yu, X. Shi, G. Yuan and J. Xie, Hierarchically structured $Co_3O_4@Pt@MnO_2$ nanowire arrays for high-performance supercapacitors, *Sci. Rep.*, 2013, **3**, 2978.

49 J. Yuan, J. Wen, Q. Gao, S. Chen, J. Li, X. Li and Y. Fang, Amorphous Co_3O_4 modified CdS nanorods with enhanced visible-light photocatalytic H_2-production activity, *Dalton Trans.*, 2015, **44**, 1680–1689.

50 J. Zhang, M. Chen and L. Zhu, Activation of persulfate by Co_3O_4 nanoparticles for orange G degradation, *RSC Adv.*, 2016, **6**, 758.

51 X. Li, S. Yang, J. Sun, P. He, X. Pu and G. Ding, Enhanced electromagnetic wave absorption performances of Co_3O_4 nanocube/reduced graphene oxide composite, *Synth. Met.*, 2014, **194**, 52–58.

52 P. K. Nayak, J. A. Caraveo-Frescas, Z. Wang, M. N. Hedhili, Q. X. Wang and H. N. Alshareef, Thin film complementary metal oxide semiconductor (CMOS) device using a single-step deposition of the channel layer, *Sci. Rep.*, 2014, **4**, 4672.

53 S. Jeong, S. Park and J. Cho, High-Performance, Layered, 3D-$LiCoO_2$ Cathodes with a Nanoscale Co_3O_4 Coating *via* Chemical Etching, *Adv. Energy Mater.*, 2011, **1**, 368–372.

54 L. Qu, K. L. Choy and R. Wheatley, An Atomistic-Scale Study for Thermal Conductivity and Thermochemical Compatibility in (DyY) Zr_2O_7 Combining an Experimental Approach with Theoretical Calculation, *Sci. Rep.*, 2015, **6**, 21232.

55 L. Zhang, W. He, X. Xiang, Y. Li and F. Li, Roughening of windmill-shaped spinel Co_3O_4 microcrystals grown on a flexible metal substrate by a facile surface treatment to enhance their performance in the oxidation of water, *RSC Adv.*, 2014, **4**, 43357.

56 M. M. Rahman, S. B. Khan, A. M. Asiri, K. A. Alamry, A. Aslam, P. Khan, A. Khan, M. A. Rub and N. Azum, Acetone sensor based on solvothermally prepared ZnO doped with Co_3O_4 nanorods, *Microchim. Acta*, 2013, **180**, 675–685.

57 O. Jankovsky, P. Simek, D. Sedmidubský, S. Huber, M. Pumera and Z. Sofer, Towards highly electrically conductive and thermally insulating graphene nanocomposites: Al_2O_3–graphene, *RSC Adv.*, 2014, **4**, 7418.

58 B. Wu, S. Zhang, F. Yao, F. Zhang and S. Xu, Synergistic lithium storage of a multi-component $Co_2SnO_4/Co_3O_4/Al_2O_3/C$ composite from a single-source precursor, *RSC Adv.*, 2015, **5**, 69932–69938.

59 J. Hou, Y. Li, M. Mao, L. Ren and X. Zhao, Tremendous effect of the morphology of birnessite-type manganese oxide nanostructures on catalytic activity, *ACS Appl. Mater. Interfaces*, 2014, **6**, 14981–14987.

60 X. Luo, W. T. Lee, G. Xing, N. Bao, A. Yonis, D. Chu, J. Lee, J. Ding, S. Li and J. Yi, Ferromagnetic ordering in Mn-doped ZnO nanoparticles, *Nanoscale Res. Lett.*, 2014, **9**, 625.

61 M. M. Rahman and J. Ahmed, Cd-doped Sb_2O_4 nanostructures modified glassy carbon electrode for efficient detection of melamine by electrochemical approach, *Biosens. Bioelectron.*, 2018, **102**, 631–636.

62 L. Nie, A. Meng, J. Yu and M. Jaroniec, Hierarchically macro-mesoporous Pt/γ-Al_2O_3 composite microspheres for efficient formaldehyde oxidation at room temperature, *Sci. Rep.*, 2013, **3**, 3215.

63 F. D. Souza, H. Fiedler and F. Nome, Zwitterionic surfactant stabilized palladium nanoparticles as catalysts in aromatic nitro compound reductions, *J. Braz. Chem. Soc.*, 2016, **27**, 372–381.

64 X. Lu, X. Bian, G. Nie, C. Zhang, C. Wang and Y. Wei, Encapsulating conducting polypyrrole into electrospun TiO_2 nanofibers: a new kind of nanoreactor for *in situ* loading Pd nanocatalysts towards p-nitrophenol hydrogenation, *J. Mater. Chem.*, 2012, **22**, 12723–12730.

65 T. Aditya, A. Palb and T. Pal, Nitroarene reduction: a trusted model reaction to test nanoparticle catalysts, *Chem. Commun.*, 2015, **51**, 9410–9431.

66 R. Y. G. König, M. Schwarze, R. Schomäcker and C. Stubenrauch, Catalytic activity of mono-and bi-metallic nanoparticles synthesized *via* microemulsions, *Catalysts*, 2014, **4**, 256–275.

67 H. Wu, L. Guo, J. Zhang, S. Miao, C. He, B. Wang, Y. Wu and Z. Chen, Polyelectrolyte-free layer by layer self-assembled multilayer films of cationic phthalocyanine cobalt(II) and carbon nanotube for the efficient detection of 4-nitrophenol, *Sens. Actuators, B*, 2016, **230**, 359–366.

68 K. Singh, A. A. Ibrahim, A. Umar, A. Kumar, G. R. Chaudhary, S. Singh and S. K. Mehta, Synthesis of CeO_2–ZnO nanoellipsoids as potential scaffold for the efficient detection of 4-nitrophenol, *Sens. Actuators, B*, 2014, **202**, 1044–1050.

69 M. Abaker, G. N. Dar, A. Umar, S. A. Zaidi, A. A. Ibrahim, S. Baskoutas and A. Al-Hajry, Effect of neutron exposure on transport of charge carriers in poly-crystalline Cu nanowires, *Sci. Adv. Mater.*, 2012, **4**, 7–8.

70 M. M. Rahman, S. B. Khan, A. M. Asiri and A. G. Al-Sehemi, Chemical sensor development based on polycrystalline gold electrode embedded low-dimensional Ag_2O nanoparticles, *Electrochim. Acta*, 2013, **112**, 422–430.

71 S. B. Khan, M. M. Rahman, K. Akhtar, A. M. Asiri, K. A. Alamry, J. Seo and H. Han, Copper oxide based polymer nanohybrid for chemical sensor applications, *Int. J. Electrochem. Sci.*, 2012, **7**, 10965–10975.

72 S. B. Khan, M. M. Rahman, K. Akhtar, A. M. Asiri and M. A. Rub, Nitrophenol chemi-sensor and active solar photocatalyst based on spinel hetaerolite nanoparticles, *PLoS One*, 2014, **9**, 85290.

73 V. A. Pedrosa, L. Codognoto and L. A. Avaca, Electroanalytical determination of 4-nitrophenol by square wave voltammetry on diamond electrodes, *J. Braz. Chem. Soc.*, 2003, **14**, 530–535.

74 M. M. Rahman, G. Gruner, M. S. Al-Ghamdi, M. A. Daous, S. B. Khan and A. M. Asiri, Chemo-sensors development based on low-dimensional codoped Mn$_2$O$_3$-ZnO nanoparticles using flat-silver electrodes, *Chem. Cent. J.*, 2013, **7**, 60.

75 M. M. Hussain, M. M. Rahman and A. M. Asiri, Efficient 2-nitrophenol chemical sensor development based on Ce$_2$O$_3$ nanoparticles decorated CNT nanocomposites for environmental safety, *PLoS One*, 2016, **11**, e0166265.

This journal is © The Royal Society of Chemistry 2018